J. Mech. Phys. Solids 186 (2024) 105597

Contents lists available at ScienceDirect

Journal of the Mechanics and Physics of Solids

journal homepage: www.elsevier.com/locate/jmps

Plastic deformations and strain hardening in fully dense granular crystals

Ashta Navdeep Karuriya, Francois Barthelat *

Department of Mechanical Engineering, University of Colorado, 427 UCB, 1111 Engineering Dr, Boulder, CO 80309, USA

ARTICLE INFO

Keywords:
Granular crystals
Granular metamaterials
Jamming
Discrete element models
Crystal plasticity

ABSTRACT

Granular crystals are intriguing constructs at the intersection between granular matter and architectured materials, offering new combinations of tunable mechanical properties, healing and recyclability. We have recently fabricated and tested strong, fully dense granular FCC crystals based on millimeter size rhombic dodecahedral grains. These "granular metamaterials" display a rich set of mechanisms: Nonlinear deformations, crystal plasticity reminiscent of atomistic mechanisms, shear-induced dilatancy, micro-buckling. Here we present discrete elements simulations of FCC granular crystals, where individual polyhedral grains are discretized with overlapping spheres. After validation with a simple cube-on-cube frictional sliding configuration, we duplicate the triaxial compression experiments on FCC granular crystals. The model captures the strength and micromechanics of deformation of the crystal but overestimates the stiffness because of imperfect contacts in the experiments. We could however use this model to identify the source of strain hardening in the crystal: Kinking of deformation bands, and collision of grains, generate strong obstacles to slip. We also show that below a certain size for the crystal, there is not enough volume to fully develop {111} frictional slip planes, which increases strength significantly. This effect can be used to increase strength by confinement, or in polycrystalline granular materials.

1. Introduction

Granular materials display unusual and interesting mechanical responses. For example, depending on confinement, they can flow like a liquid or be as stiff and strong as a solid (Jaeger et al., 1996). They also show a rich set of mechanisms: jamming, shear bands, clusters formation, localized regions of stress transfer, shear-induced dilatation (Behringer and Chakraborty, 2018; Radjai et al., 2017). However, as structural materials, the inherent randomness and poor packing of typical granular materials limits their mechanical performance. Granular materials are usually based on spherical or ellipsoidal grains (Behringer and Chakraborty, 2018; Radjai et al., 2017) which leads to sub-optimal load transfer between individual grains of poor packing. For example, the packing factor (solid volume fraction) for randomly arranged spheres is only 0.55 to 0.64 (Onoda and Liniger, 1990) which is significantly smaller than ideal volume fraction in closed packed spheres (0.74) which is itself much smaller than a perfect packing (packing factor=1). The poor packing in typical granular materials causes suboptimal load transfer: applied mechanical loads are channeled along thin "force chains lines" that occupy only a small fraction in the material while most grains remain free of stress (Behringer et al., 2014). A possible route to enhance mechanical responses and properties is by controlling the shape of the individual grains (Brown et al., 2010; Wang et al., 2021). For example, granular materials based on cubical, tetrahedral and octahedral grains are 40 to 80 % stronger than the traditional

* Corresponding author.
E-mail address: francois.barthelat@colorado.edu (F. Barthelat).

https://doi.org/10.1016/j.jmps.2024.105597
Received 3 August 2023; Received in revised form 22 February 2024; Accepted 26 February 2024
Available online 29 February 2024
0022-5096/Published by Elsevier Ltd.

spheroid-based granular materials, because of limited grain rotations and increasing jamming (Athanassiadis et al., 2014). However, the arrangement of these grains is random, which still limits the packing density and mechanical properties. Another approach to enhance mechanical response is to order the grains into "granular crystals". Crystallization in granular materials can indeed be induced with careful choice of particle shape, container geometry and mechanical stimulus including shearing or mechanical vibration (Roth and Jaeger, 2016; Villarruel et al., 2000). Crystallization in granular materials can induce unusual properties and mechanical responses. For example, one-dimensional granular chains and granular crystals display unusual and useful characteristics in terms of elastic wave propagation, acoustics, or shock waves attenuation (Daraio et al., 2006; Hascoët et al., 1999; Porter et al., 2015). "Topologically interlocked materials (TIMs)" are panels made of interlocking blocks, which can be described as a two-dimensional granular crystals (Estrin et al., 2021, 2011). Controlled grain sliding and geometrical hardening give rise to controlled deformability and impact resistance (Bahmani et al., 2022; Dyskin et al., 2003; Mirkhalaf et al., 2018; Siegmund et al., 2016). We have recently designed and fabricated nearly fully dense "granular crystals" with millimeters-size grains (Karuriya and Barthelat, 2023) that combine the concepts of TIMs, granular mechanics and three-dimensional crystallization. Triaxial compression tests showed that these granular crystals are up to 25 times stronger than randomly packed spheres (Karuriya and Barthelat, 2023). They also displayed a rich set of mechanisms: Nonlinear deformations, crystal plasticity reminiscent of atomistic mechanisms, geometrical hardening, cross-slip, shear-induced dilatancy, micro-buckling. While theoretical models could capture the onset of yielding in FCC granular crystals, we have yet to explain the pronounced strain hardening observed experimentally. A possible route to explore these mechanisms is the discrete element method (DEM) first introduced by Cundall (Cundall and Strack, 1979) and now commonly used to model granular systems with sphere-on-sphere contacts (Zhou et al., 2017). Modeling granular crystals using DEM however presents special challenges: (i) the grains are non-spherical and (ii) flat-on-flat contact forces are governed not only on the penetration distance, but also on the surface area and sliding distance between the grains. For non-spherical systems involving flat-on-flat contacts, various modeling approaches have been proposed which can also take into account the sliding distance between the grains (Feng, 2023; Kawamoto et al.,

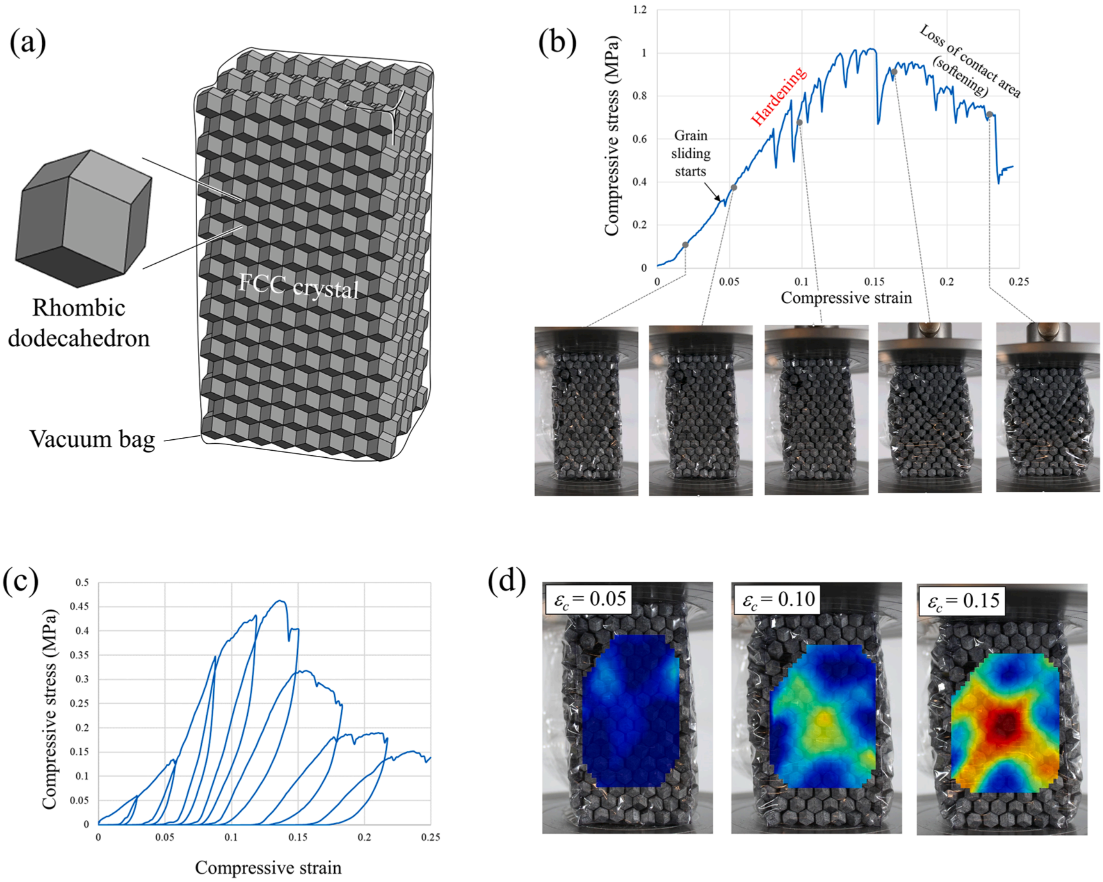

Fig. 1. (a) A space-filling ~800-grains granular crystal made from rhombic dodecahedral grains confined with a vacuum bag; (b) Experimental compressive stress-strain curve showing yielding, strain hardening and softening (confining pressure = 60 kPa). Snapshots of the sample show "granular crystal plasticity" along well-defined slip planes; (c) Cycling of the crystal at increasing levels of strains show that the deformations are "plastic", with residual strains upon unloading (confining pressure = 30 kPa); (d) Local maximum shear strain $\gamma_{\max}$ computed from individual grain tracking, at three level of applied compressive strain ε_c. A "X" pattern of two deformation bands develops, with the highest strains at the intersection of the deformation bands.

2018, 2016; Lu et al., 2015). One of such approaches is to discretize individual grains into overlapping spheres (Garcia et al., 2009; Kruggel-Emden et al., 2008; Li et al., 2015; Salerno et al., 2018), which can be easily implemented, and with a level of accuracy that can be tuned with the number and density of spheres (Nguyen and Plimpton, 2019; Thompson et al., 2022). Another method is based on level sets and the discretization of grains with nodes to capture the mechanics of grains with arbitrary shapes (Kawamoto et al., 2018), or even to capture the mechanics of TIMs with a large number of flat-on-flat contacts (Koureas et al., 2023).

In this paper we first summarize our previous experimental results on granular FCC crystals, and we discuss possible strain hardening mechanisms. We then discuss the overlapping sphere DEM model in the context of a sliding flat contact with a two-cube model, and we then apply this model to large FCC granular crystals. Finally, we use the model to elucidate the main sources of strain hardening, and to explore the effect of crystal size on strain delocalization and plastic confinement.

2. Face centered cubic (FCC) granular crystals: Structure and mechanical response

This section briefly describes the face centered cubic (FCC) granular crystals loaded in the "off-axis" direction, which is the focus of the present study. In our previous work (Karuriya and Barthelat, 2023) we fabricated fully dense FCC granular crystals (Fig. 1a) by placing rhombic dodecahedral grains inside a rectangular container subjected to high-amplitude vibrations. The grains were confined in a vacuum bag and interacted only by dry frictional contact. We performed triaxial compression tests on these crystals following standards procedure from soil mechanics (Powrie, 2018). The grains were first confined with a vacuum bag, and then subjected to uniaxial compression. These tests showed that these granular crystals are up to 25 times stronger than randomly packed spheres (Karuriya and Barthelat, 2023). Fig. 1b shows a typical response from an off-axis compression test. The front face of the sample is a {111} plane, and the crystal is loaded in compression along the off-axis direction $<\overline{1}\overline{1}2>$. In that loading direction an elastic region is rapidly followed by an initial yield point where grains start to slide on one another along two intersecting slip planes in the crystal (Fig. 1b, 1d). The initial yielding point for the crystal is marked by the onset of sliding between the grains, which we identified by image analysis and tracking of the individual grains (Karuriya and Barthelat, 2023). The initial yielding is followed by massive strain hardening and by sudden unloading-reloading probably related to stick-slip or "micro-avalanches" in the crystal. The reloading slope is much greater than the initial slope, indicating that initially the contact between the grains may be imperfect leading to low stiffness, but that pressure on the system brings the grains closer to a full contact configuration that leads to much greater overall stiffness. We refer to this deformation mechanism as "granular crystal plasticity" because of analogies with traditional crystal plasticity. Fig. 1c shows a stress-strain curve with unloading-reloading cycles at different level of deformations. These unloading cycles show evidence of residual plastic strains, and they also show that the "yielding" of the crystal occurs at low stresses and strains, the increase of stress with deformation being therefore attributed to strain hardening. Competing with strain hardening is a softening mechanism from the progressive loss of surface area between the sliding grains. This competition leads to a maximum stress, followed by strain softening. A striking feature of this response is the massive strain hardening observed after the initial yield point. This behavior is in stark contrast with traditional granular materials, which typically form one or only a few localized shear bands with strain softening as soon as the strength is reached (Behringer and Chakraborty, 2018).

While the onset of yielding can be accurately captured using a "granular crystal plasticity" model inspired from classical crystal plasticity (Karuriya and Barthelat, 2023), the source of strain hardening in this granular crystal is unknown and more difficult to pinpoint. Full strain fields can provide insights into this mechanism. Fig. 1d shows maps of the local maximum shear strains for three levels of applied compressive strains (the strains were computed using a grain-tracking algorithm from the experimental images). These maps reveal two deformation bands which increase in intensity and width as the compression increases. These bands intersect forming a "X pattern", with the highest levels of strains at the intersection between the bands. Based on these experimental

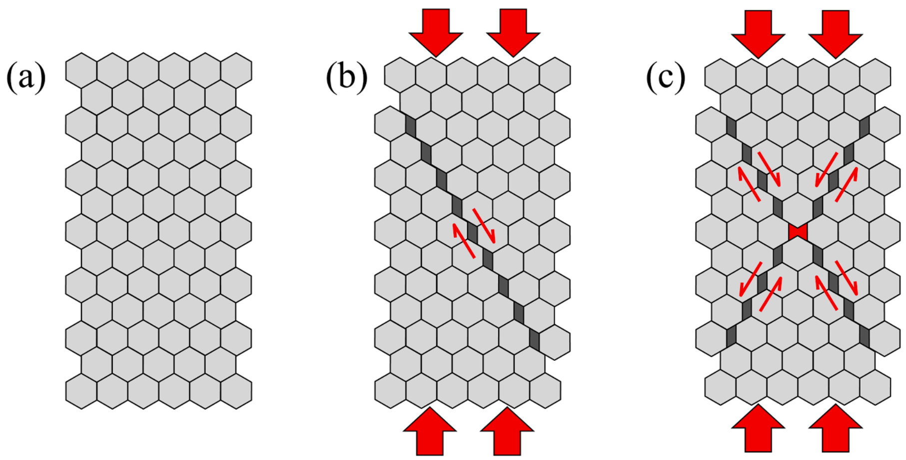

Fig. 2. Possible micromechanics of granular crystal plasticity: (a) Initial configuration; (b) Single slip plane activated, where shear and dilation dominate; (c) Two intersecting slip planes are activated. Compression jamming can occur at the intersection between the slip planes (in red).

observations, we propose potential sources of strain hardening in the granular crystal on Fig. 2. The first possible hardening mechanism considered a single activated slip plane in 2D or 3D, with the intuition that the applied compression would increase confinement, thereby frustrating the dilation associated with shearing to lead to strain hardening (Fig. 2b). Modeling the force transfer across that single band, however, failed to predict any strain hardening from this mechanism. The morphology of the grains and the surface of the slip plane indeed induce dilation, which can be interpreted as the slip occurring along a "partial dislocation" vector. The resolved shear stress is indeed lower along that direction, which means that the compressive strength is increased. However, no hardening is generated, and softening instead occurs because of the loss of contact area. Fig. 2c illustrates another potential hardening mechanism: Two intersecting slip planes form an "X pattern" as seen in the experiments (Fig. 1d). In terms of kinematics, the slip planes partition the material into four sectors which can be considered rigid for the purpose of the model. As highlighted in red on Fig. 2c, the upper and lower regions collide at the intersection of the slip planes, generating a "compressive jamming" of grains. Another possible hardening mechanism is the formation of kinks along the shear bands at their intersection point. These kinks could provide a geometrical obstacle to slip along each of the bands, which may be strong enough to generate strain hardening. To explore these mechanisms in detail and in three-dimensions is challenging and requires numerical tools, which we present in the following sections.

3. Overlapping sphere models for a pair of sliding cubes

In typical granular materials made of convex grains, the contact force and contact areas between individual grains are governed only by the shape of the grains and the interpenetration distance (geometrical interference) between the grains. In addition, if the grains are stiff then the contact area is small relative to the size of the grain, and as a result stresses and strains are localized near the contact points. In contrast, densely packed polyhedral grains involve large flat-on-flat contact areas which evolve with sliding, and which are more difficult to capture in models. The contact areas are larger and in the order to the size of the grains, and the contact forces and contact areas depend not only on the penetration distance, but also on the sliding distance between the grains. To illustrate these effects, consider two cubes of size $l \times l \times l$ each (Fig. 3a). The cubes are positioned so that one of their faces is in full contact, with a compression pre-strain ε_0 so that the distance between the centers of mass of the two cubes is set to $l(1\text{-}\varepsilon_0)$. We assume that the cubes are linear elastic (modulus E) and that frictional contact is governed by Coulomb friction with friction coefficient f. For a pair of sliding ($u > 0$) homogenous cubes, the normal and tangential forces are given by:

$$\begin{cases} P = El^2\varepsilon_0\left(1 - \frac{u}{l}\right) \\ T = fP \end{cases} \tag{1}$$

Eq. (1) are plotted on Fig. 3b, with all forces normalized by the initial compression force $P_0 = El^2\varepsilon_0$. This solution, verified experimentally in (Dalaq and Barthelat, 2019), highlights the main features of the elastic contact of sliding blocks with finite sizes: (i) Normal and tangential forces are higher for higher pre-compression strains (i.e. higher confinement) and (ii) These forces are the highest when the cubes are in full contact ($u = 0$) but when the cubes slide and the contact area decreases, the volume of the cube deformed elastically, decrease and as a result normal and tangential forces decrease linearly with sliding distance until the cubes lose contact entirely.

These flat-on-flat contact interactions require a numerical contact law that not only accounts for the penetration distance between two grains (as typical DEM codes do), but also the contact area between the grains. One approach is to discretize the contact surface with overlapping spheres (Garcia et al., 2009; Kruggel-Emden et al., 2008; Li et al., 2015) as shown on Fig. 4 for the case of a cube. We use two parameters to control the density and arrangement of the spheres: The numbers of spheres desired on each edge N_e, and the

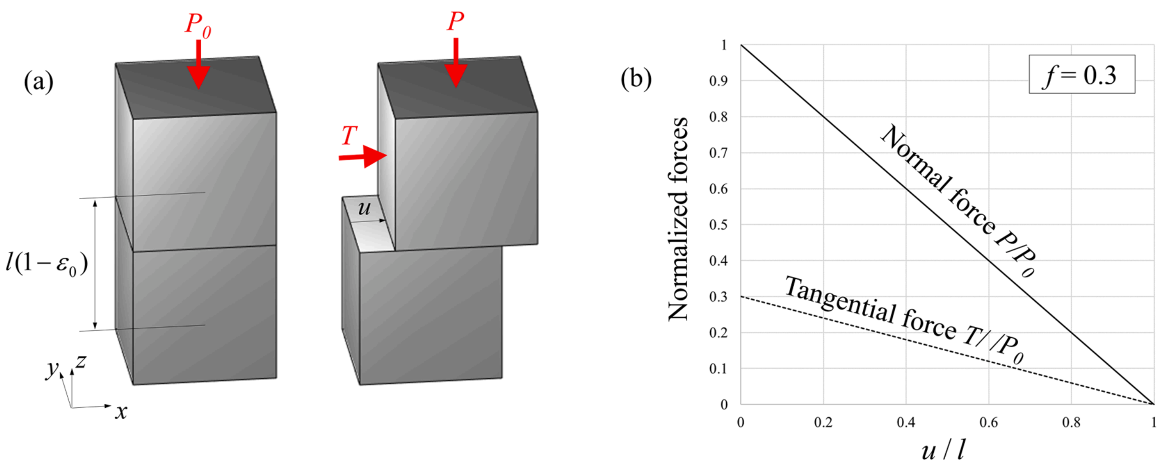

Fig. 3. Theoretical response for the frictional sliding of two elastic cubes in contact: (a) The cubes are subjected to a precompression strain ε_0 which is held constant during sliding; (b) Predicted normal and tangential forces as function of sliding distance. The forces are normalized by $P_0 = El^2\varepsilon_0$.

overlap between the spheres κ. We require that (i) the spheres are tangential to the flat faces of the cube, which requires the centers of the spheres to be recessed from the faces of the grain surface by a distance $d/2$ where d is the diameter of the spheres and (ii) spheres be equally spaced on the edges. These requirements lead to the required diameter of the spheres:

$$\frac{d}{l} = \frac{1}{(N_e - 1)(1 - \kappa) + 1} \tag{2}$$

Once these discretization parameters are set on the edges of the cubes, we use a Delaunay triangularization approach to mesh the entire surface of the cube. Fig. 4 shows that tuning N_e and κ leads to a great variety of possible models, the overlapping sphere model becoming "smoother" for higher N_e and for higher κ.

Spheres within the same grain can overlap but they do not interact, and their relative positions are fixed. Spheres belonging to different grains do interact through a specified contact law. Since the contact of these sphere is supposed to represent the elastic deformation of the block, we used a simple linear Hooke's law for the contact:

$$p = k_n \delta \tag{3}$$

Where p is the normal contact force between a pair of spheres, k_n is the contact stiffness between individual spheres and δ is the geometrical interference between a pair of spheres (i.e., the penetration distance). The contact law between the spheres must then be calibrated to match the response of a homogenous and continuous cube. If the positions of the spheres across the contact surface of the cube coincide, then the contact stiffness of the surface in the normal direction is equal to the sum of the contact stiffnesses for the individual sphere-on-sphere contacts. The compressive force can then be written:

$$P = N_f k_n \delta = \left(N_f k_n l\right) \varepsilon_0 \tag{4}$$

Where N_f is the number of spheres on an individual face of the cube. Comparing Eq. (4) and (1) for $u = 0$ gives the "in-line" sphere stiffness:

$$k_n = \frac{El}{N_f} \tag{5}$$

Using the areal density of the spheres $\rho_s \approx \frac{N_f}{l^2}$, Eq. (5) can be written:

$$k_n \approx \frac{E}{\rho_s l} \tag{6}$$

In summary, the individual spheres follow a linear contact model which only depends on the penetration distance. However, the stiffness of the flat surfaces discretized with multiple spheres is more complex and is also a function of the sliding distance: as the two cubes slide on one another the number of spheres in contact decreases, which decreases the contact stiffness of the flat contact area. Eq. (6) provides the contact stiffness based on a conformation where the positions of the spheres across the contact surface coincide, but this is not the case in general: During sliding contact the position of the sphere in one cube shifts relative to the spheres of the other cube, so the normal contact forces between the spheres may no longer be perpendicular to the face of the cube. The main hypothesis of the overlapping sphere model is that the in-plane components of the individual forces cancel each other over an average taken over a

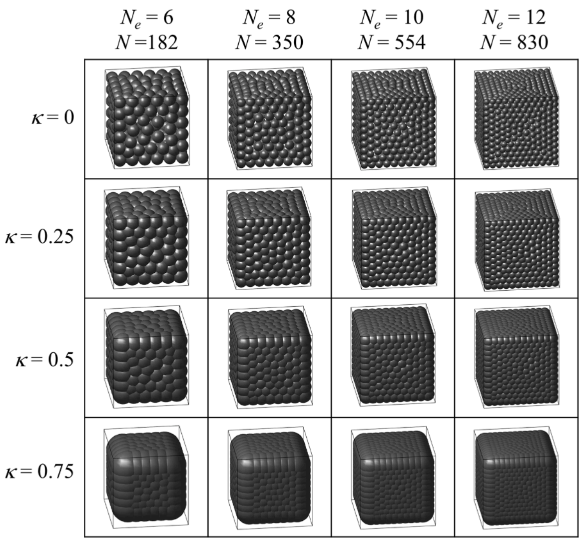

Fig. 4. Discretization of cubes with overlapping spheres using various combinations for the number of spheres on the edge N_e and for the sphere overlap κ. The resulting total number of sphere N is also shown. For all cases the spheres are tangential to the theoretical faces of the grains.

sufficiently large number of spheres, and that the sum of the components over a large enough number of spheres can be used to represent a net contact force across the surface. To verify this hypothesis, we modeled two cubes in contact using overlapping spheres (Fig. 5a), using the granular package in LAMMPS (Thompson et al., 2022). For each cube, a wall in the horizontal x-y plane was used to maintain the compressive pre-strain ε_0 between the cubes, and a set of walls in the vertical y-z plane was used to impose sliding and to prevent rotation of the cubes. Each set of walls was moved along the x direction in opposed direction to generate a controlled sliding distance u (Fig. 5a). LAMMPS uses the explicit Verlet integration method based on time integration, and therefore we made sure to select a loading rate, the mass of the individual spheres and the time stepping to be all sufficiently small to achieve quasi-static equilibrium (this aspect is discussed further below, for the case of the granular crystals). Fig. 5b shows the normalized normal and tangential forces as function of sliding displacements for the case of zero friction. Overall, the contact forces properly decreased linearly with sliding distance (Fig. 5b), in accordance with the theoretical model. For $u = 0$ the DEM model matched the theoretical response, but for $u > 0$ the DEM model underestimates the normal force: The x-y positions of the spheres from the two cubes and across the contact surface do not match anymore, and as a result the apparent stiffness of the discretized surface is lower than the theoretical model. The DEM model also shows fluctuations due to the discrete events of breaking and reforming contacts as the two cubes slide. Refining the discretization (higher N_e and κ) can however reduce these fluctuations, which brought the DEM predictions closer to the theoretical model. The model also examines the possibility that the discretized surface creates an artificial frictional force (even for $f = 0$) because of the "artificial roughness" created and the in-plane components of sphere-on-sphere contact forces. Fig. 5b shows that this effect does indeed generate fluctuations in the tangential force T, but that these fluctuations remain small and oscillate about $T = 0$. Finally, Fig. 5c shows results for two sliding cubes with friction. A history-dependent frictional law was used in LAMMPS (Brilliantov et al., 1996; Silbert et al., 2001; Zhang and Makse, 2005), with a coefficient of friction of $f = 0.3$. This local frictional law is properly reflected at the level of the cube face, with $T = fP$ (plus/minus fluctuations associated with the sphere-based discretization). To summarize we find that the overlapping sphere tends to underestimate the stiffness of the cubes in a flat-on-flat sliding contact configuration. We did not attempt to obtain contact stiffness closer to the theoretical model, because as we show in the next sections the actual contact stiffness between grains in a granular crystal is much lower than the theoretical value, due to imperfections in the contact forces. The discretization also generates some fluctuations in forces, which can be decreased by refining the model. The overlapping sphere models however captures two critical features well: The contact forces decrease when the contact area decreases

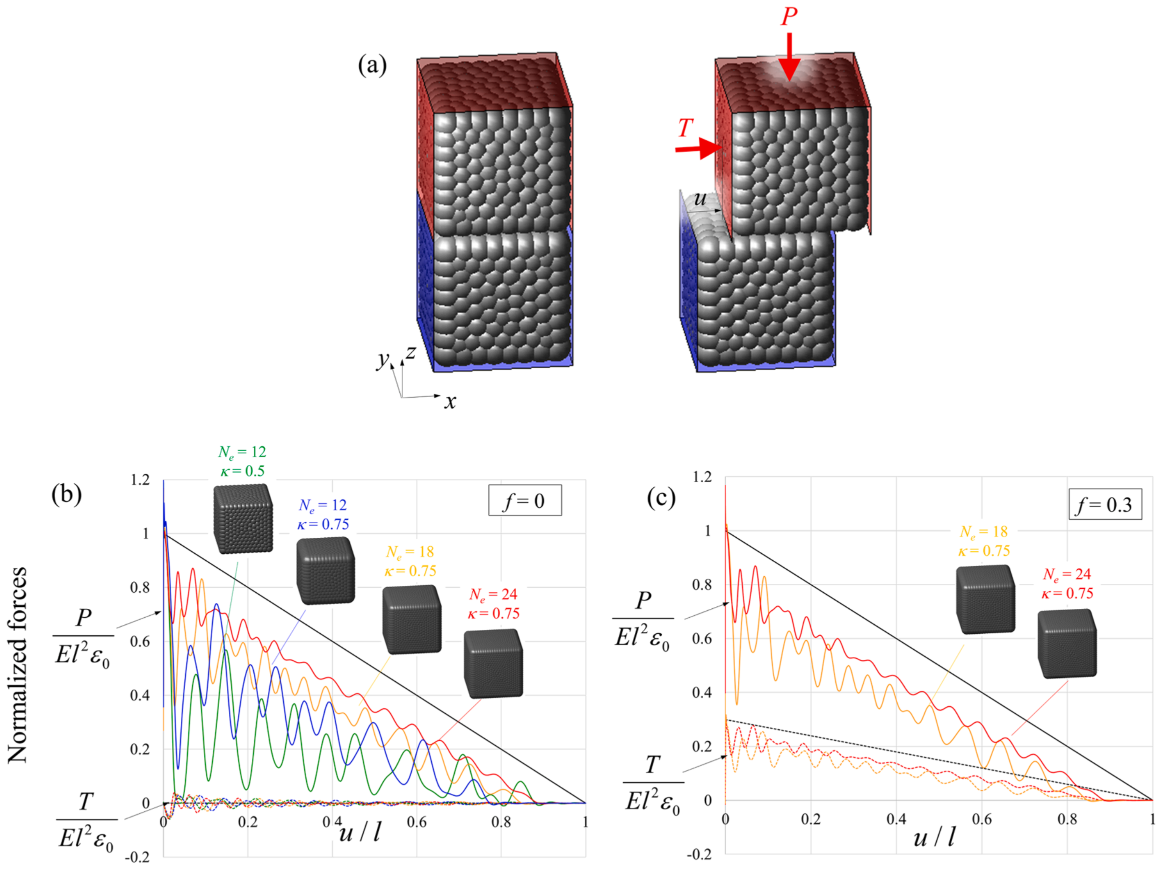

Fig. 5. DEM model for two sliding cubes: (a) two discretized cubes are held by walls (in blue and red) which are used to generate controlled sliding; Normalized normal force P and tangential forces T for (b) zero friction and (c) friction = 0.3. The results for various levels of discretization are shown for each case, together with the theoretical response.

(which will lead to softening in the granular crystal), and the modeled tangential force accurately reflects Coulomb friction. This modeling tool can therefore be useful to predict the flow of contact forces and patterns of frictional sliding in a granular crystal.

4. Modeling fully dense FCC granular crystals

We now apply the overlapping sphere DEM model to fully dense FCC granular crystals. In fully dense FCC granular crystals, the individual grains are rhombic dodecahedra with a size a that matches the size of the unit cell (Fig. 6a). We discretized the individual rhombic dodecahedral grains with N_e spheres on the edges and a sphere overlap κ. As described above we require the spheres to be tangential to the flat faces of the grain, which for the rhombic dodecahedron leads to the required diameter of the spheres:

$$d = \frac{a}{\frac{4}{\sqrt{3}}(N_e - 1) + \sqrt{2}} \tag{7}$$

As for the two-cube model above, we assumed a linear contact law between individual spheres, with contact stiffness k_n. A possible general course of action for the modeling of granular materials is to use k_n as fitting parameter so the predictions of the model at the macroscale match the experimental data at the macroscale (Kawamoto et al., 2018). In this study we took a different route, where we calculate k_n from the modulus E of the grains, which we measured experimentally (E_g=3 GPa (Karuriya and Barthelat, 2023)). We then used Eq. (6) applied to the dodecahedron:

$$k_n \approx \frac{E_g}{\rho_s a} \tag{8}$$

Where ρ_s is the areal density of the spheres, which depend on the chosen discretization level N_e. In the experiment the grains were subjected to a hydrostatic pressure p_0 using a vacuum bag at three different pressures (p_0 =10, 30 or 60 kPa). In the model this was achieved by pre-straining the crystal by a compressive hydrostatic pre-strain ε_0 by creating the crystal using unit cell size $(1 - \varepsilon_0)a$, and by applying the corresponding hydrostatic pressure p_0 to the outer grains in the model (Fig. 6c). This pressure was applied by subjecting the individual surface grains to forces proportional to p_0 and to the surface area of their projection on the surface of the crystal. As a second step, uniaxial compression was applied along the long axis of the crystal, using two horizontal walls obeying the same contact law as the sphere-on-sphere contacts (Fig. 6d), including friction which implied that the grains could slide along the loading platforms. The walls were brought together at a slow rate in order to compress the model, and the corresponding compressive forces were determined by summing all contact forces between the grains and the walls. An important step was to ensure that the discretization of the grains was fine enough for convergence, and to ensure that the loading rate and mass of the grains produced a quasi-static equilibrium at each loading step. Fig. 7a shows a series of compressive stress-strain curves for different combinations of the discretization parameters N_e and κ. In these simulations we used the same properties and parameters as in the experiments: Modulus of the individual grain $E_g = 3$ GPa, coefficient of friction between grains $f = 0.35$ (measured experimentally (Karuriya and Barthelat, 2023)), and confining pressure $p_0 = 60$ kPa. The overall shape of the curve is relatively uniform across different grain discretization, although details differ. All curves show an initial yield point, followed by strain hardening, a peak stress and then softening. The initial yield stress and maximum stress is roughly independent from N_e and κ in the range of values shown here, but finer discretization (larger N_e and κ) lead to smoother curves. Fig. 7b shows the apparent compressive strength of the crystals, measured as a reaction force on the upper surface of the crystal (in red) and on the lower surface of the crystal (in blue), both plotted as function of a non-dimensional loading rate $L\dot{\varepsilon}/\sqrt{E/\rho}$where L is the length of the crystals, $\dot{\varepsilon}$ is the compressive strain rate, E is the modulus of the crystal and ρ its mass density (used for mass scaling). For high loading rate and/or high mass density dynamic effects lead to higher apparent compressive strengths, and to cases where the upper and lower reaction forces are different from one another (i.e. the model is not in static equilibrium). As the loading rate is decreased and/or the mass density is decreased, the apparent strength of the crystal

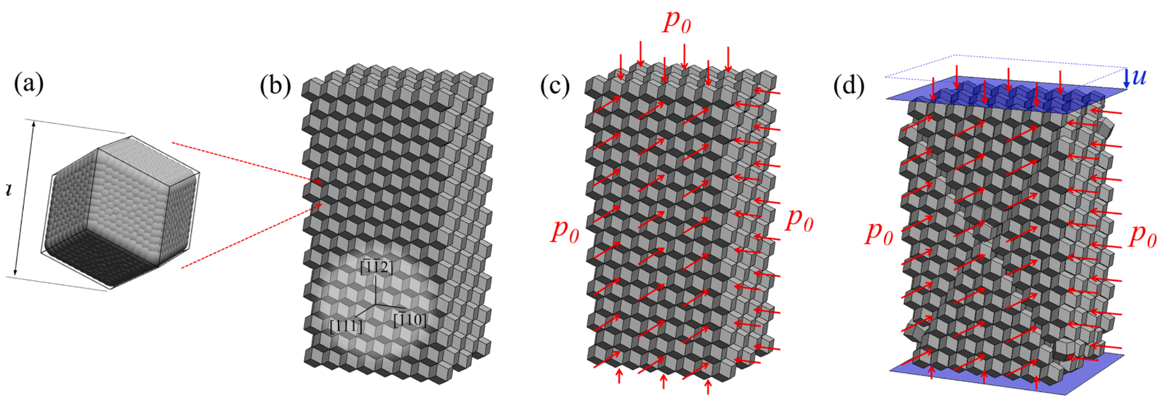

Fig. 6. DEM model of a granular crystal: (a) A rhombic dodecahedral grain of size a is discretized with spheres; (b) 864 grains are arranged in a FCC lattice with unit cell size a and "off-axis" orientation; (c) a hydrostatic compression p_0 is first applied to duplicate the effect of the vacuum bag in the experiments; (d) uniaxial compression is applied using walls (in blue).

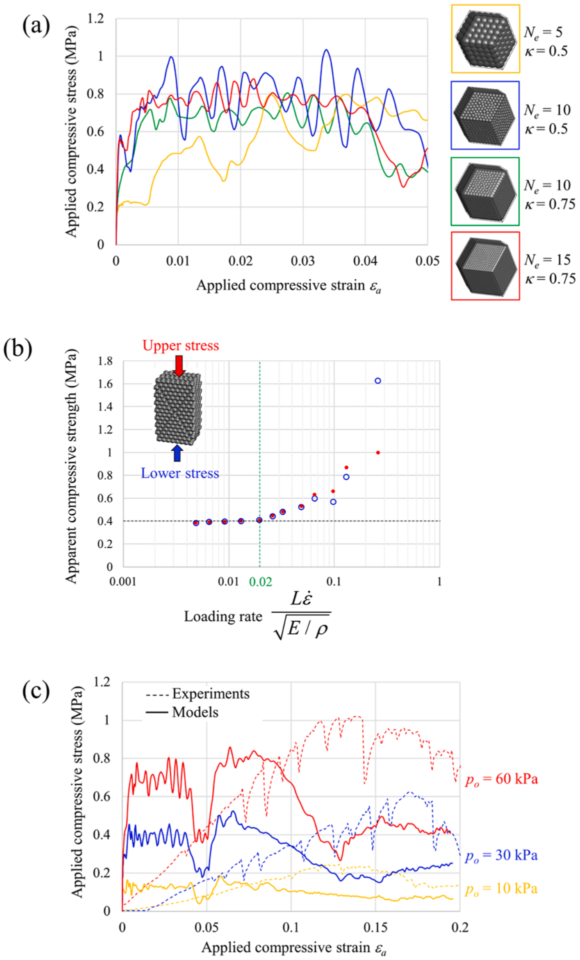

Fig. 7. (a) Simulated compressive stress-strain curves for four different levels of grain discretization; (b)the apparent compressive strength of the crystals, measured as a reaction force on the upper surface of the crystal (in red) and on the lower surface of the crystal (in blue), both plotted as function of a non-dimensional loading rate $L\dot{\varepsilon}/\sqrt{E/\rho}$where L is the length of the crystals, $\dot{\varepsilon}$ is the compressive strain rate, E is the modulus of the crystal and ρ its mass density (used for mass scaling). (c) comparison with experiments for three levels of confining pressure.

decreases. For $L\dot{\varepsilon}/\sqrt{E/\rho}<0.02$ the apparent strength is no longer sensitive to rate and mass, and the two reaction forces are identical, which indicates that a quasi-static state of equilibrium was achieved in the model. We therefore used $L\dot{\varepsilon}/\sqrt{E/\rho}=0.02$ for all simulations (including for the simulations shown on Fig. 7a). Finally, we used a small damping value for normal and tangential contact forces to ensure stability, but also ensuring that damping was small enough not to alter the compressive forces. In summary the compressive stress-strain curves presented here are converged and do not depend on timestep, loading rate, mass and damping. Fig. 7c shows the compressive stress-strain curves predicted for p_0 =10, 30 and 60 kPa and for N_e =10 and κ = 0.75, with comparisons with the experimental results. The model captures the sequence of yielding-hardening-softening in the experiments, and it also captures the effect of the confining pressure p_0. The predicted initial yield strength and ultimate strength for the crystal are remarkably close to the experiments. Moreover, the model predicts that the initial yield strength is proportional to the confining pressure p_0, which is expected since the initial sliding of the grains is governed by Coulomb friction. The predicted yield strength can be written $\sigma_y \sim 7p_0$ for $f = 0.35$, which is remarkably close to prediction from the 3D granular crystal plasticity model we have recently developed (Karuriya and Barthelat, 2023). While the numerical model predicts the proper overall response and stress levels appropriately, the level of overall deformation and modulus for the crystal are several times higher than the experiments. We attribute this discrepancy to the assumption of perfect contact in the model, where the contact stiffness was computed from the modulus of the material of which they are made of. In the reality of experiments, the contacts are imperfect because of surface roughness, grain misalignment or small variations in individual grain size which results in thin gaps at the interfaces. As a result, the overall experimental stiffness of the crystal is much lower than predicted by the model. In addition, the model assumes perfect contact between the loading platforms and the crystal, whereas in the experiments, uneven contacts and nonperfect alignments may lead to lower apparent modulus for the crystal. We have not attempted to capture these imperfections in the numerical model (although we note that in the experiments, the short unloading-reloading events due to stick slip show reloading moduli which are closer to the models).

Importantly, the DEM simulations provide the position and rotation of each grain in the crystal, making it a valuable tool to explore the micromechanics of deformation. Fig. 8 shows a stress- strain curve predicted with a p_0=60 kPa confinement, together with snapshots of three different sections of the model (*A, B, C*) taken at five different levels of deformations. The mechanism that dominates nonlinear deformations is slip along two intersecting planes forming a "X pattern", which is consistent with the experiments (Fig. 1d). Slip initiates by frictional sliding along {111} planes in the crystal, but the geometry of the sample and the loading conditions steer the pattern towards a series of partial {111} slip planes along the diagonal planes of the samples. These deformations along specific slip planes in the material are reminiscent of classical crystal plasticity at the atomic scale. In our granular crystals however, the interaction between individual grains is relatively stiff, which leads to a dislocation width larger than the size of the crystals. As a result, we did not observe any dislocation in the experiments and in the model, and instead the grains underwent a collective shift along the slip planes. The deformation pattern is therefore partly governed by microstructure, loading condition and sample geometry which is typical of system where the scale of the structure approaches the size of the sample and where separation of scale is not possible (Similar issues arise in lattice materials (Bertoldi et al., 2017) and topological interlocked materials (Dyskin et al., 2003; Siegmund, 2011)). In addition, we colored the grains according to the "severity" of the contact forces, which we calculated using the following procedure: We first computed, for each grain, the sum Δ of the penetration distance from their neighboring grains. We then computed $\overline{\Delta}$ the grain penetration averaged over the entire volume of the model. Fig. 8 shows the normalized grain-level penetration $\Delta/\overline{\Delta}$. In each snapshot,

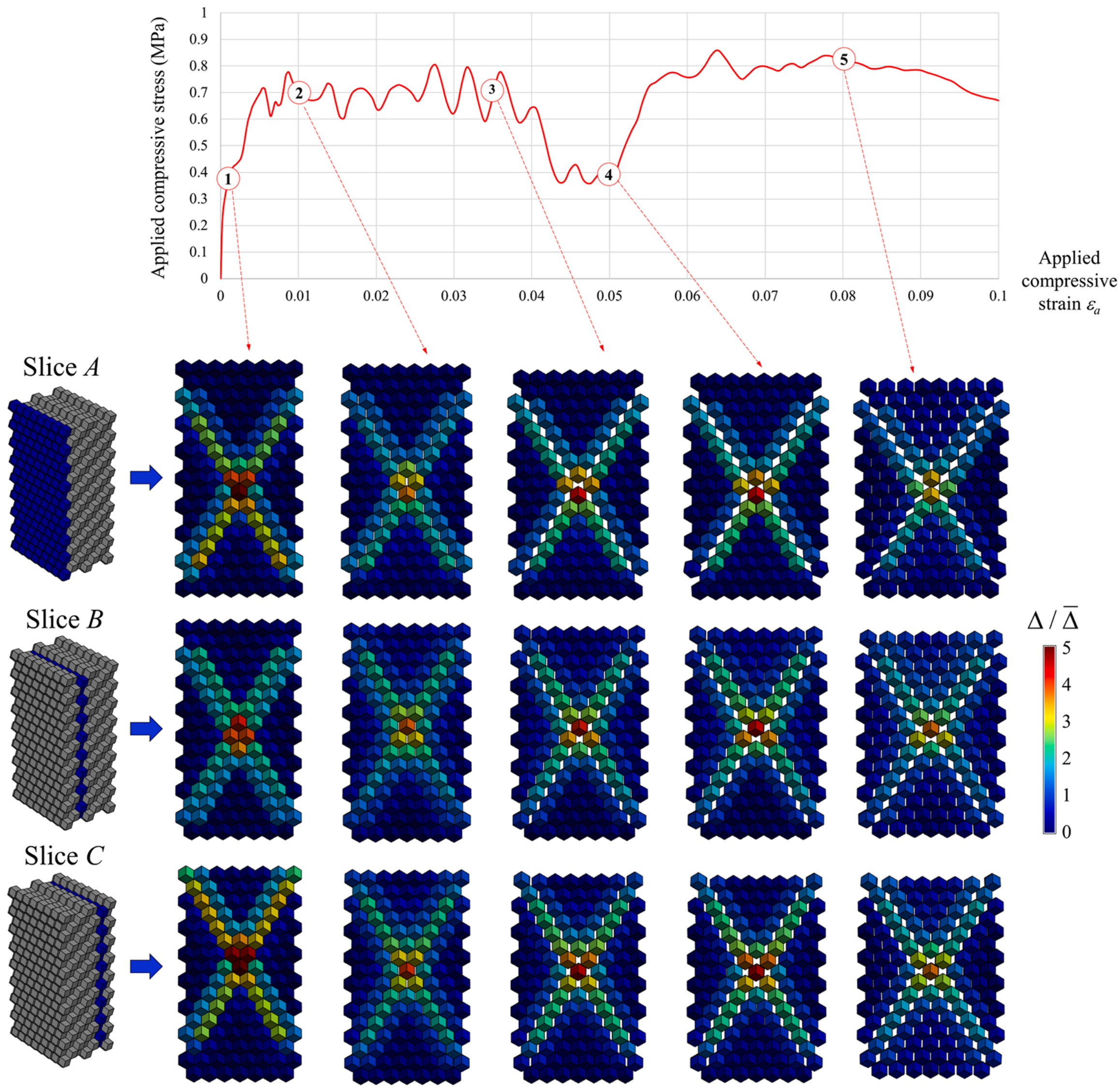

Fig. 8. Predicted compressive stress-strain curve with details of the micromechanics in three sections of the model (*A, B, C*). For each snapshot, the color shows the "severity" of the contact $\Delta/\overline{\Delta}$ is shown where Δ is the sum of the penetration distance for each grain and $\overline{\Delta}$ is the grain penetration averaged over the volume of the model.

$\Delta/\overline{\Delta}$ is the highest along the X-shape deformation bands, the highest values occurring at the intersection of these bands.

Fig. 9 highlights how concentrated contact forces at the intersection between the deformation bands can give rise to hardening. Fig. 9a and 9b show the details of slice *C*, where a kink forms in each of the deformation at the intersection with the other band. The larger penetration distance in these areas suggests that these kinks generate a geometrical obstacle to shearing, which can lead to strain hardening. Hardening competes with the progressive loss of contact area between the grains and at a strain of about 0.04 (Fig. 8) the stress decreases, but this is shortly followed by a second strain hardening mechanism: Fig. 9c shows a snapshot of slice *A* in the second hardening region, showing that a set of grains near the center of the crystal, initially not in contact, are collide after the collapse of the deformation bands. This secondary collision of grains creates high compressive stresses, which stabilizes the deformation bands and leads to a sustained stress at the macroscale.

5. Knockout (KO) models

The results of the previous section strongly suggest that hardening mechanisms occur at the intersection between the slip planes, in accordance with the hypothesis developed in Section 1. To prove this mechanism, we simply removed ("knocked out") the grains which are expected to be at the intersection of the slip planes, and we assessed the effects on the stress-strain curves. Fig. 10 shows the results from these numerical experiments. Removing fifteen grains in the center of the sample and through the thickness (where the intersect between slip planes is expected) effectively removes a major obstacle to shearing of the slip planes (Fig. 10c). Compared to the full reference model (blue curve on Fig. 10a), this KO model results in a decrease of compressive strength (initial yield strength and maximum strength), and to softening starting relatively early on the stress-strain curves (red curve on Fig. 10a). Taken from other places in the crystal, this removal has much less effect. Knocking out 15 grains on one of the slip planes results in a drop of strength of less than 10 % (Fig. 10c, orange curve), and knocking out 15 grains outside of the slip regions results in even smaller changes in the stress strain curves (Fig. 10c, light blue and green curves).

6. Strain delocalization in larger granular crystals

In the previous sections we showed how kinking of shear band and grain collision at the intersection of the slip planes generates strain hardening, in the form of increasing stress with strain. The effect of hardening on strain delocalization could however not be clearly seen in the experiments and in the models, because of geometric confinement: The full activation of slip planes in the crystal requires the entire periphery of the slip plane to intersect free boundaries (or at least deformable boundaries). Slip planes that intersect the loading platform cannot therefore be activated, which we hypothesized could limit the extent of plastic deformation in the crystal, even in the presence of pronounced strain hardening. We verified this hypothesis by compressing crystals with a higher aspect ratio. Fig. 11 shows the results from models at three different aspect ratios (AR). AR=2 is the reference crystal discussed in the previous section. As discussed above, the crystal only develops two intersecting slip planes along $\{2\overline{1}\overline{1}\}$ planes. Fully formed {111} slip planes are not possible because of the geometrical confinement imposed by the loading platforms. Doubling the aspect ratio to AR=4 leads to a different response. The initial yield strength is identical, but the stress-strain curve shows less hardening and less fluctuations. Snapshots taken at different strain levels show that the first yield point coincides with the formation of fully developed {111} slip planes in the volume of the crystal (Fig. 11b). Strain hardening rapidly leads to the creation of additional slip planes and the thickening of the deformation bands. The final snapshots of Fig. 11 show that at large strains the crystal is saturated with plastic deformation. To appreciate this unusual response, it is useful to again recall the typical triaxial response of randomly distributed granular materials, where large deformations localize in one, or a few shear bands. Crystals with higher aspect ratio (AR=4) therefore allow fully {111} slip plane to develop and propagate over the entire available volume of crystals. It is then expected than in contrast, reducing the AR

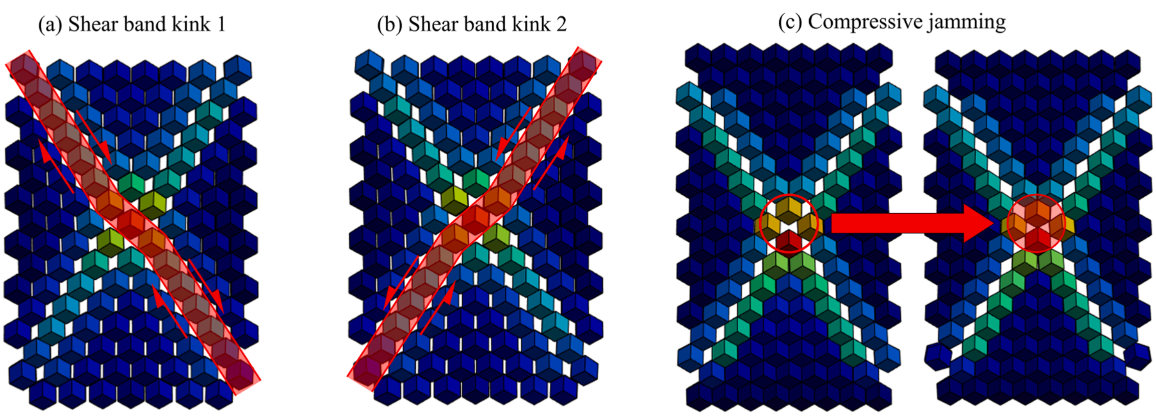

Fig. 9. Snapshots from Fig. 8, used to highlight (a-b) a primary strain hardening mechanism, where kinks on the deformation bands create geometrical obstacles to slip; (c) a secondary hardening mechanism, where groups of grains, initially far from one another, collide after the collapse of the deformation bands.

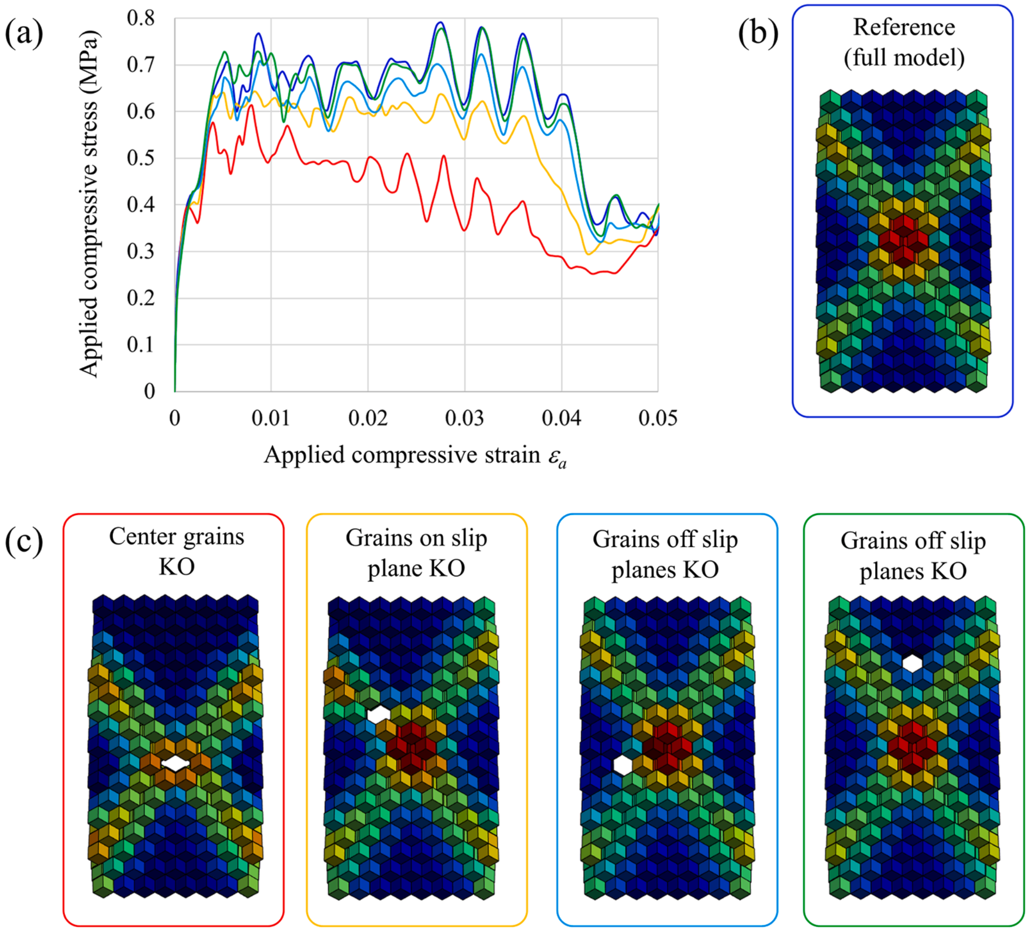

Fig. 10. Intersections of slip plane are key to strain hardening and strength: (a) Compressive stress-strain curves color coded: (b) Reference model (blue); (c) Knocked out (KO) models: (Red): Model with the 15 center grains at the intersection of the slip planes knocked out though the thickness of the model, resulting in early softening and low strength; (Orange): 15 grains on the expected slip plane knocked out; (light blue and green): 15 grains off the slip planes knocked out, with minimal effect on strength.

from 2 should impede the formation of any slip plane, forcing the activation of other deformations mechanisms and possibly leading to higher strength. Indeed, models of short crystals (AR=1) show the same elastic modulus as the longer crystals, but their initial strength is 3–4 times greater and their ultimate strength up to 7 times greater. Snapshots show a relatively uniform distribution of deformations, where all grains are forced to slide simultaneously with no apparent slip plane or localization. This deformation mode requires a much larger stress to activate, leading to significantly higher strength.

Finally, we validated these observations with experiments. We fabricated granular crystals with aspect ratio AR=1,2 and 4, using the same grains and fabrication methods as we previously used (Karuriya and Barthelat, 2023). Fig. 12 shows that the compressive strength increases as the length of the crystal (AR) was reduced, in accordance with the model. For the reference crystal (AR=2), {111} slip planes do not form due to geometrical confinement imposed by the loading platform, and grains simply slide mostly on two intersecting $\{2\overline{1}\overline{1}\}$ planes. On the other hand, snapshots taken on the longer AR=4 crystal (Fig. 12b) confirm the formation of full {111} slip planes along wide bands which progressively propagate throughout the volume of the crystal. The yield strength is identical with AR=2, but we observed less hardening in the stress-strain curve. Experiments also confirmed that reducing the length of the crystal to AR = 1 forbade the formation of any slip planes, instead showing homogenous grain sliding with no apparent slip plane or localization, in consistent with the model.

7. Conclusions

Fully dense granular crystals are a relatively new type of architectured materials (or “granular metamaterials”) which are substantially stronger than traditional, randomly distributed granular materials. They display intriguing deformation mechanisms akin to classical crystal plasticity, with specific slip planes activated by compressive stress. While the onset of yield is well understood and can be captured with a frictional granular plasticity model (Karuriya and Barthelat, 2023), strain hardening, and the sequence of slip plane

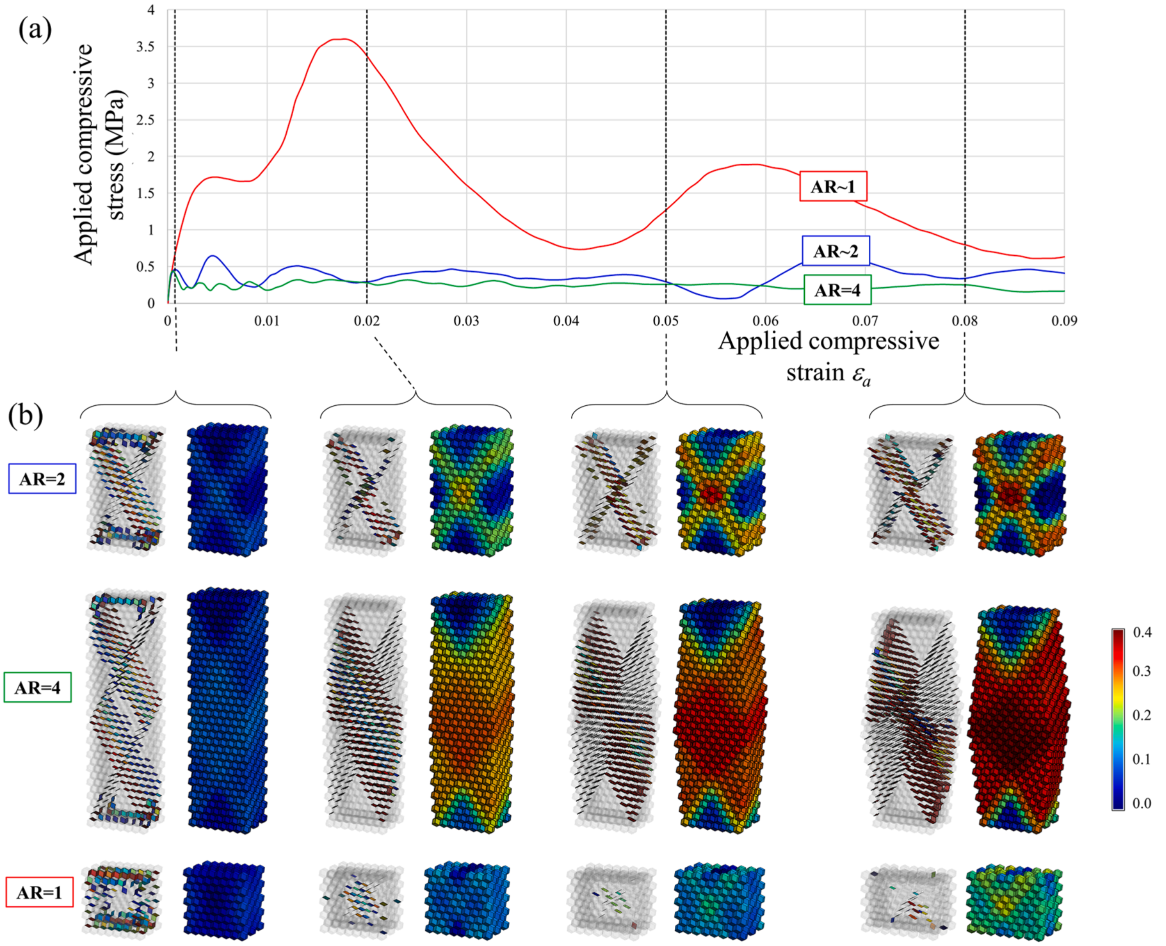

Fig. 11. Effect of confinement on granular plasticity, DEM models: (a) Compressive stress strain curves for granular crystals with three aspect ratios (AR=1,2,4). (b) Snapshots at four strain levels: Interfaces with a sliding distance greater than 2 times the average sliding, along with local equivalent strain. Confining pressure is p_0= 30 kPa for all models.

formation was so far not understood. Here we have used discrete element models where each grain is approximated with overlapping spheres to investigate these questions. The main findings are summarized below:

- We show, using two cubes in contact, that the overlapping sphere model can capture flat-on-flat fictional sliding contacts, including softening due to loss of contact area.
- This modeling approach can capture nonlinear deformation mechanisms in large granular FCC crystals made of rhombic dodecahedral grains. Modeling individual grains with about 1000 overlapping spheres yielded converged results in terms of stresses and strains.
- With independently measured properties and no curve fitting involved, the model properly captured the experimental initial yield strength and ultimate strength, as well as the effect of confining pressure on these properties.
- The model overestimated the elastic modulus of the crystal by a large amount, because it assumes perfect contact between the grains. We explain this discrepancy by the imperfect contact between the grains in the experiments.
- For a crystal with aspect ratio AR =2, two slip planes develop in the crystal, in accordance with experimental observations. The initial yield strength is consistent with experiments and with our previously developed “granular crystal plasticity” model (Karuriya and Barthelat, 2023).
- A primary strain hardening mechanism occurs from the kinking of deformation bands at the regions where the bands intersect. These kinks generate strong geometrical obstacles to slip along the deformation bands.
- A secondary primary strain hardening mechanism occurs at larger strains, where the collapse of the initial deformation bands creates new contact between the grains, which stabilize the material and generates strength over larger strains.
- Models with those grains at the intersection of slip planes knocked out showed strain softening instead of strain hardening, which confirms the hardening mechanisms that occur at these regions.

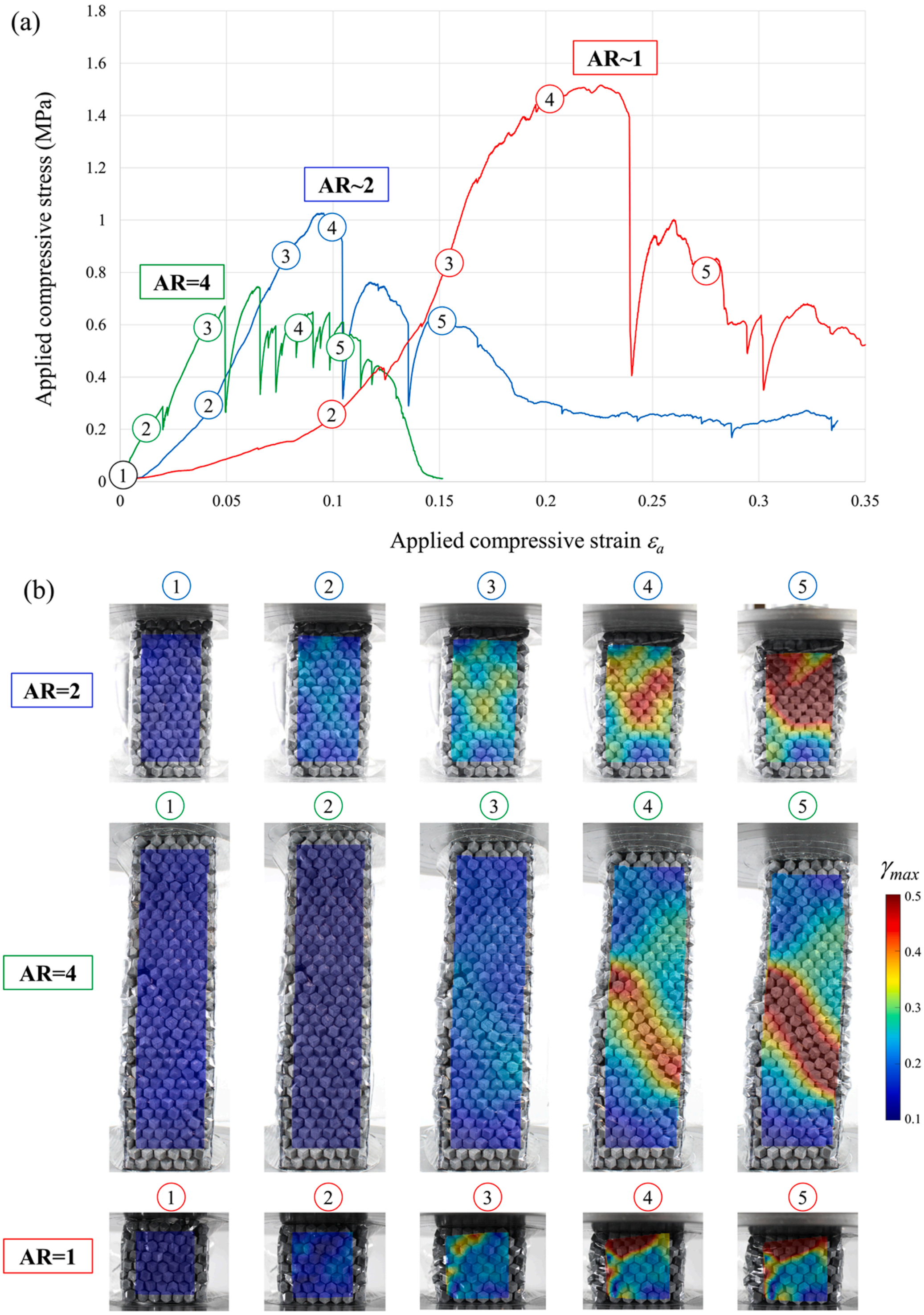

Fig. 12. Effect of confinement on granular plasticity, experiments: (a) Compressive stress strain curves for granular crystals with three aspect ratios (AR=1,2,4). (b) Snapshots at five strain levels, overlaid with the contours for maximum shear strain obtained from digital image correlation. Confining pressure is p_0= 30 kPa for all experiments.

- Experiments and models both showed that long FCC crystals (AR=4) developed fully formed {111} slip planes that propagated throughout the entire available volume. In this larger model, strain hardening enabled delocalization of strains, the available volume of the crystal eventually getting saturated with plastic deformation.

- Experiments and models both showed that short crystals (AR=1) were too confined to activate any slip plane. Instead, this configuration led to uniform and homogenous sliding of the grains which required more stress, and which therefore led to strength 3–7 higher than longer crystals.

A drawback of the model is that it did not capture the stiffness of the crystal accurately, which we attributed to imperfect contacts between individual grains in the experiments. In the future the contact law may be refined to include these imperfections by using non-linear contact laws, or by incorporating defects such as local misorientation of grains or grains with non-planar faces. These additional features would require careful calibrations from independent experiments and characterization, so that these more complex models do not devolve into curve-fitting exercises. Nevertheless, the overlapping sphere models presented here provide a powerful modeling platform to capture strength and mechanics of deformation in FCC granular crystals. In the future, this model can be used to explore other types of crystals (BCC, HCP) and other loading conditions or to explore the effect of imperfections such as grain boundaries or vacancies. The model could also be used to tailor and optimize the interfaces between the grains. For example, we verified with our model that using higher coefficient of friction leads to higher overall strength. Other features at the interfaces, such as adhesion or specific rheologies, could be used to generate attractive mechanical response for the crystal. Granular crystals are unusual materials, and they present interesting features, for example fully dense granular crystals could be used as a recyclable modular structural material made from “universal” building blocks that can be recycled an indefinite number of times, and these materials could be easily repaired, reshaped, or altered on-site. They could also be used for impact protection or energy dissipation because of their combinataion of stiffness, mechanical stability, strength and large deformations.

CRediT authorship contribution statement

Ashta Navdeep Karuriya: Data curation, Formal analysis, Investigation, Methodology, Validation, Visualization, Writing – original draft, Writing – review & editing. **Francois Barthelat:** Conceptualization, Data curation, Formal analysis, Funding acquisition, Investigation, Methodology, Project administration, Resources, Software, Supervision, Validation, Visualization, Writing – original draft, Writing – review & editing.

Declaration of competing interest

The authors declare that they have no known competing financial interests or personal relationships that could have appeared to influence the work reported in this paper.

Data availability

Data will be made available on request.

Acknowledgments

This work was sponsored by the University of Colorado Boulder and by the Army Research Office under Grant Number: W911NF-21–1–0175. The views and conclusions contained in this document are those of the authors and should not be interpreted as representing the official policies, either expressed or implied, of ARO or the U.S. Government. The U.S. Government is authorized to reproduce and distribute reprints for Government purposes notwithstanding any copyright notation herein.

References

Athanassiadis, A.G., Miskin, M.Z., Kaplan, P., Rodenberg, N., Lee, S.H., Merritt, J., Brown, E., Amend, J., Lipson, H., Jaeger, H.M., 2014. Particle shape effects on the stress response of granular packings. Soft Matter 10, 48–59. https://doi.org/10.1039/C3SM52047A.

Bahmani, A., Pro, J.W., Hannard, F., Barthelat, F., 2022. Vibration-driven fabrication of dense architectured panels. Matter 5, 899–910. https://doi.org/10.1016/j.matt.2022.01.002.

Behringer, R.P., Bi, D., Chakraborty, B., Clark, A., Dijksman, J., Ren, J., Zhang, J., 2014. Statistical properties of granular materials near jamming. J. Stat. Mech. 2014, P06004. https://doi.org/10.1088/1742-5468/2014/06/P06004.

Behringer, R.P., Chakraborty, B., 2018. The physics of jamming for granular materials: a review. Rep. Prog. Phys. 82, 012601 https://doi.org/10.1088/1361-6633/aadc3c.

Bertoldi, K., Vitelli, V., Christensen, J., van Hecke, M., 2017. Flexible mechanical metamaterials. Nat Rev. Mater 2, 1–11. https://doi.org/10.1038/natrevmats.2017.66.

Brilliantov, N.V., Spahn, F., Hertzsch, J.M., Pöschel, T., 1996. Model for collisions in granular gases. Phys. Rev. E 53, 5382–5392. https://doi.org/10.1103/PhysRevE.53.5382.

Brown, E., Rodenberg, N., Amend, J., Mozeika, A., Steltz, E., Zakin, M.R., Lipson, H., Jaeger, H.M., 2010. Universal robotic gripper based on the jamming of granular material. Proceed. Nat. Acad. Sci. 107, 18809–18814. https://doi.org/10.1073/pnas.1003250107.

Cundall, P.A., Strack, O.D.L., 1979. A discrete numerical model for granular assemblies. Géotechnique 29, 47–65. https://doi.org/10.1680/geot.1979.29.1.47.

Dalaq, A.S., Barthelat, F., 2019. Strength and stability in architectured spine-like segmented structures. Int. J. Solids Struct. 171, 146–157. https://doi.org/10.1016/j.ijsolstr.2019.04.012.

Daraio, C., Nesterenko, V.F., Herbold, E.B., Jin, S., 2006. Energy trapping and shock disintegration in a composite granular medium. Phys. Rev. Lett. 96, 058002 https://doi.org/10.1103/PhysRevLett.96.058002.

Dyskin, A.V., Estrin, Y., Kanel-Belov, A.J., Pasternak, E., 2003. Topological interlocking of platonic solids: a way to new materials and structures. Philos Mag Lett 83, 197–203. https://doi.org/10.1080/0950083031000065226.

Estrin, Y., Dyskin, A.V., Pasternak, E., 2011. Topological interlocking as a material design concept. Mater. Sci. Eng. 31, 1189–1194. https://doi.org/10.1016/j.msec.2010.11.011.

Estrin, Y., Krishnamurthy, V.R., Akleman, E., 2021. Design of architectured materials based on topological and geometrical interlocking. J. Mater. Res. Techn. 15, 1165–1178. https://doi.org/10.1016/j.jmrt.2021.08.064.

Feng, Y.T., 2023. Thirty years of developments in contact modelling of non-spherical particles in DEM: a selective review. Acta Mech. Sin. 39, 722343 https://doi.org/10.1007/s10409-022-22343-x.

Garcia, X., Latham, J.P., Xiang, J., Harrison, J.p., 2009. A clustered overlapping sphere algorithm to represent real particles in discrete element modelling. Géotechnique 59, 779–784. https://doi.org/10.1680/geot.8.T.037.

Hascoët, E., Herrmann, H.J., Loreto, V., 1999. Shock propagation in a granular chain. Phys. Rev. E 59, 3202–3206. https://doi.org/10.1103/PhysRevE.59.3202.

Jaeger, H.M., Nagel, S.R., Behringer, R.P., 1996. Granular solids, liquids, and gases. Rev. Mod. Phys. 68, 1259–1273. https://doi.org/10.1103/RevModPhys.68.1259.

Karuriya, A.N., Barthelat, F., 2023. Granular crystals as strong and fully dense architectured materials. Proceed. National Acad. Sci. 120, e2215508120 https://doi.org/10.1073/pnas.2215508120.

Kawamoto, R., Andò, E., Viggiani, G., Andrade, J.E., 2018. All you need is shape: predicting shear banding in sand with LS-DEM. J Mech Phys Solids 111, 375–392. https://doi.org/10.1016/j.jmps.2017.10.003.

Kawamoto, R., Andò, E., Viggiani, G., Andrade, J.E., 2016. Level set discrete element method for three-dimensional computations with triaxial case study. J Mech Phys Solids 91, 1–13. https://doi.org/10.1016/j.jmps.2016.02.021.

Koureas, I., Pundir, M., Feldfogel, S., Kammer, D.S., 2023. Beam-like topologically interlocked structures with hierarchical interlocking. J Appl Mech 90, 081008. https://doi.org/10.1115/1.4062348.

Kruggel-Emden, H., Rickelt, S., Wirtz, S., Scherer, V., 2008. A study on the validity of the multi-sphere discrete element method. Powder Technol 188, 153–165. https://doi.org/10.1016/j.powtec.2008.04.037.

Li, C.Q., Xu, W.J., Meng, Q.S., 2015. Multi-sphere approximation of real particles for DEM simulation based on a modified greedy heuristic algorithm. Powder Technol 286, 478–487. https://doi.org/10.1016/j.powtec.2015.08.026.

Lu, G., Third, J.R., Müller, C.R., 2015. Discrete element models for non-spherical particle systems: from theoretical developments to applications. Chem. Eng. Sci. 127, 425–465. https://doi.org/10.1016/j.ces.2014.11.050.

Mirkhalaf, M., Zhou, T., Barthelat, F., 2018. Simultaneous improvements of strength and toughness in topologically interlocked ceramics. Proceed. National Acad. Sci. 115, 9128–9133. https://doi.org/10.1073/pnas.1807272115.

Nguyen, T.D., Plimpton, S.J., 2019. Aspherical particle models for molecular dynamics simulation. Comput Phys Commun 243, 12–24. https://doi.org/10.1016/j.cpc.2019.05.010.

Onoda, G.Y., Liniger, E.G., 1990. Random loose packings of uniform spheres and the dilatancy onset. Phys. Rev. Lett. 64, 2727–2730. https://doi.org/10.1103/PhysRevLett.64.2727.

Porter, M.A., Kevrekidis, P.G., Daraio, C., 2015. Granular crystals: nonlinear dynamics meets materials engineering. Phys Today 68, 44–50. https://doi.org/10.1063/PT.3.2981.

Powrie, W., 2018. Soil mechanics: concepts and applications, 3rd Edition. CRC Press.

Radjai, F., Roux, J.N., Daouadji, A., 2017. Modeling granular materials: century-long research across scales. J. Eng. Mech. 143, 04017002 https://doi.org/10.1061/(ASCE)EM.1943-7889.0001196.

Roth, L.K., Jaeger, H.M., 2016. Optimizing packing fraction in granular media composed of overlapping spheres. Soft Matter 12, 1107–1115. https://doi.org/10.1039/C5SM02335A.

Salerno, K.M., Bolintineanu, D.S., Grest, G.S., Lechman, J.B., Plimpton, S.J., Srivastava, I., Silbert, L.E., 2018. Effect of shape and friction on the packing and flow of granular materials. Phys. Rev. E 98, 050901. https://doi.org/10.1103/PhysRevE.98.050901.

Siegmund, T., 2011. Heterogeneous topologically interlocked materials: a new class of heterogeneous materials. Advances in Heterogeneous Material Mechanics, p. 0, 2011.

Siegmund, T., Barthelat, F., Cipra, R., Habtour, E., Riddick, J., 2016. Manufacture and mechanics of topologically interlocked material assemblies. Appl. Mech. Rev. 68, 040803 https://doi.org/10.1115/1.4033967.

Silbert, L.E., Ertaş, D., Grest, G.S., Halsey, T.C., Levine, D., Plimpton, S.J., 2001. Granular flow down an inclined plane: bagnold scaling and rheology. Phys. Rev. E 64, 051302. https://doi.org/10.1103/PhysRevE.64.051302.

Thompson, A.P., Aktulga, H.M., Berger, R., Bolintineanu, D.S., Brown, W.M., Crozier, P.S., in 't Veld, P.J., Kohlmeyer, A., Moore, S.G., Nguyen, T.D., Shan, R., Stevens, M.J., Tranchida, J., Trott, C., Plimpton, S.J., 2022. LAMMPS - a flexible simulation tool for particle-based materials modeling at the atomic, meso, and continuum scales. Comput. Phys. Commun. 271, 108171 https://doi.org/10.1016/j.cpc.2021.108171.

Villarruel, F.X., Lauderdale, B.E., Mueth, D.M., Jaeger, H.M., 2000. Compaction of rods: relaxation and ordering in vibrated, anisotropic granular material. Phys. Rev. E 61, 6914–6921. https://doi.org/10.1103/PhysRevE.61.6914.

Wang, Y., Li, L., Hofmann, D., Andrade, J.E., Daraio, C., 2021. Structured fabrics with tunable mechanical properties. Nature 596, 238–243. https://doi.org/10.1038/s41586-021-03698-7.

Zhang, H.P., Makse, H.A., 2005. Jamming transition in emulsions and granular materials. Phys. Rev. E 72, 011301. https://doi.org/10.1103/PhysRevE.72.011301.

Zhou, W., Yang, L., Ma, G., Xu, K., Lai, Z., Chang, X., 2017. DEM modeling of shear bands in crushable and irregularly shaped granular materials. Granular Matter 19, 25. https://doi.org/10.1007/s10035-017-0712-y.